

Understanding Substituent Effects on ^{29}Si Chemical Shifts and Bonding in Disilenes. A Quantum Chemical Analysis[†]

Dominik Auer, Carsten Strohmann,* Alexei V. Arbuznikov, and Martin Kaupp*

Institut für Anorganische Chemie, Universität Würzburg,
Am Hubland, 97074 Würzburg, Germany

Received February 12, 2003

The ^{29}Si chemical shift tensors in both symmetrically and unsymmetrically substituted disilenes have been analyzed by quantum chemical calculations. A detailed breakdown of the paramagnetic contributions to nuclear shielding into individual sum-over-states terms allows new insights into the interrelations between bonding and chemical shifts in these unsaturated compounds. While the substituent effects in symmetrically substituted systems may be understood to a large extent from the energy denominators of the perturbation expression, the very different shifts for the two silicon nuclei in unsymmetrically substituted systems are mainly due to the spatial extent and orientation of the occupied and unoccupied molecular orbitals, as sampled by the matrix elements of nuclear magnetic moments at both silicon sites. The unequal shifts may thus be understood and could serve as a diagnostic tool to distinguish between symmetrically and unsymmetrically substituted disilenes. Furthermore, unequal charge transfer and an alternating charge distribution can rationalize unexpectedly larger pyramidalization of the silyl-substituted silicon center in unsymmetrically substituted systems.

Introduction

Since the discovery of the first stable disilene, tetramesityldisilene,¹ in the early 1980s, a variety of differently substituted systems have been synthesized.^{2–12} The preparation of such double-bonded silicon systems still poses a great challenge to the synthetically working chemist. In particular, unsymmetrically substituted systems are complicated to obtain, and therefore only a few examples have been described so far.^{4,7,10,11} The bonding situation in compounds of this type has been investigated by various methods, including crystal structure analysis, UV/vis spectroscopy, and liquid and solid-state NMR spectroscopy.^{2,4–17} Of the applied ana-

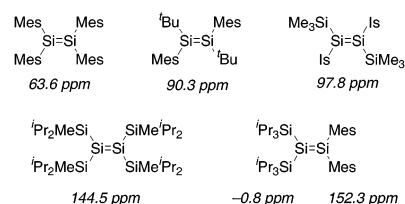


Figure 1. ^{29}Si NMR shifts of selected disilenes (Mes = 2,4,6-trimethylphenyl, Is = 2,4,6-triisopropylphenyl).

lytical methods, ^{29}Si NMR spectroscopy has frequently been the method of choice. Indeed, solid-state ^{29}Si NMR has provided not only isotropic shift values but also the detailed shift tensors.¹⁷ The observed chemical shift (CS) values of symmetrical disilenes may be classified by the substitution pattern around silicon and fall in distinct ranges: 56.2–66.5 ppm (aryl-substituted disilenes),^{2,4,6,7,13–17} 87.1–96.9 ppm (mixed aryl/alkyl systems),^{2,5,9,15} 94.2–97.8 ppm (mixed aryl/silyl systems),^{5,6,17} and 141.9–154.5 (silyl systems).^{8,10,17}

The experimentally determined shift tensors encode important electronic structure information. However, due to the complexity of the shift tensor, the relation to structure and bonding is not easy to establish and requires usually explicit quantum chemical analyses. To understand the observed chemical shifts (CS) in

[†] Dedicated to Professor Wolfgang Malisch on the occasion of his 60th birthday.

* Corresponding authors. E-mail: c.strohmann@mail.uni-wuerzburg.de, kaupp@mail.uni-wuerzburg.de.

- (1) West, R.; Fink, M. J.; Michl, J. *J. Science* **1981**, *214*, 1343.
- (2) Michalczyk, M. J.; West, R.; Michl, J. *J. Am. Chem. Soc.* **1984**, *106*, 821.
- (3) Michalczyk, M. J.; West, R.; Michl, J. *Organometallics* **1985**, *4*, 826.
- (4) Yokelson, H. B.; Siegel, D. A.; Millevolte, A. J.; Maxka, J.; West, R. *Organometallics* **1990**, *9*, 1005.
- (5) Archibald, R. S.; Van den Winkel, Y.; Millevolte, A. J.; Desper, J. M.; West, R. *Organometallics* **1992**, *11*, 3276.
- (6) Tokitoh, N.; Suzuki, H.; Okazaki, R.; Ogawa, K. *J. Am. Chem. Soc.* **1993**, *115*, 10428.
- (7) Weidenbruch, M.; Pellmann, A.; Pan, Y.; Pohl, S.; Saak, W.; Marsmann, H. *J. Organomet. Chem.* **1993**, *450*, 67.
- (8) Kira, M.; Maruyama, T.; Kabuto, C.; Ebata, K.; Sakurai, H. *Angew. Chem.* **1994**, *106*, 1575.
- (9) Shepherd, B. D.; Powell, D. R.; West, R. *Organometallics* **1989**, *8*, 2664.
- (10) Kira, M.; Ohya, S.; Iwamoto, T.; Ichinohe, M.; Kabuto, C. *Organometallics* **2000**, *19*, 1817.
- (11) Ichinohe, M.; Arai, Y.; Sekiguchi, A.; Takagi, N.; Nagase, S. *Organometallics* **2001**, *20*, 4141.
- (12) Wiberg, N.; Niedermayer, W.; Noth, H.; Warchhold, M. *Z. Anorg. Allg. Chem.* **2001**, *627*, 1717.

(13) Wiberg, N.; Niedermayer, W.; Polborn, K. *Z. Anorg. Allg. Chem.* **2002**, *628*, 1045.

(14) Zilm, K. W.; Grant, D. M.; Michl, J.; Fink, M. J.; West, R. *Organometallics* **1983**, *2*, 193.

(15) Fink, M. J.; Michalczyk, M. J.; Haller, K. J.; Michl, J.; West, R. *Organometallics* **1984**, *3*, 793.

(16) Yokelson, H. B.; Siegel, D. A.; West, R. *J. Am. Chem. Soc.* **1986**, *108*, 4239.

(17) West, R.; Cavalieri, J. D.; Buffy, J. J.; Fry, C.; Zilm, K. W.; Duchamp, J. C.; Kira, M.; Iwamoto, T.; Mueller, T.; Apeloig, Y. *J. Am. Chem. Soc.* **1997**, *119*, 4972.

disilenes, quantum chemical calculations have been performed by some authors.^{11,17} The proper basis for interpretation is provided by Ramsey's equation¹⁸ (eq 1), i.e., by second-order perturbation theory (unless relativistic effects become important¹⁹). Except for proton NMR, it is usually assumed that changes in chemical shifts are due to changes in paramagnetic shielding, σ^p :²⁰

$$\sigma_N^p = \frac{1}{2c^2} \sum_{n \neq 0} \frac{\langle \Psi_n | L_O | \Psi_0 \rangle \cdot \langle \Psi_0 | L_N \cdot r_N^{-3} | \Psi_n \rangle}{E_0 - {}^1E_n} + c.c. \quad (1)$$

Here, Ψ_0 and Ψ_n are the many-electron wave functions of the ground and n th excited singlet state, respectively, and E_0 and 1E_n provide the corresponding energies. The two matrix elements in the numerators reflect interactions with (a) the external magnetic field ("orbital Zeeman term", OZ) and with (b) the magnetic moment of the nucleus in question (the paramagnetic-nuclear-spin-electron-orbit term, PSO).²⁰

West et al.¹⁷ related the main substituent effects on isotropic ²⁹Si shifts to the most deshielded component (σ_1) of the shielding tensor and attributed the changes to the energy denominator of the sum-over-states expression in eq 1, more precisely to the interaction between the ground state and the $\sigma(\text{Si}=\text{Si}) \rightarrow \pi^*(\text{Si}=\text{Si})$ excited state. Experimentally determined ²⁹Si NMR shifts of various symmetrically substituted disilenes appear to confirm this behavior, for example when one compares alkyl- and aryl-substituted systems ($\delta^{29}\text{Si}$ 56.2–96.9 ppm) with tetrasilyl-substituted compounds ($\delta^{29}\text{Si}$ 141.9–154.5 ppm). West et al. suggested that electropositive substituents decrease the $\Delta E(\sigma \rightarrow \pi^*)$ values and therefore increase σ^p .¹⁷

However, this argument may not be used to explain shieldings in unsymmetrically substituted disilenes. While the unsymmetrical, but only aryl-substituted, disilene $(\text{Mes})_2\text{Si}=\text{Si}(\text{Is})_2$ (Is = 2,4,6-triisopropylphenyl) exhibits almost identical ²⁹Si NMR shifts (57.9, 59.4 ppm) for both silicon centers, the unsymmetrically substituted compound $(\text{Pr}_3\text{Si})_2\text{Si}=\text{Si}(\text{Mes})_2$ ¹¹ shows a very large difference between the ²⁹Si NMR chemical shifts of the two central silicon atoms ($(\text{Pr}_3\text{Si})_2\text{Si}=\text{Si}(\text{Mes})_2$: 152.3 ppm for $(\text{Mes})_2\text{Si}$; -0.8 ppm for $(\text{Pr}_3\text{Si})_2\text{Si}$; further examples see ref 21]. The reasons for these "... Unusual ²⁹Si NMR Chemical Shifts ..." (title of ref 11) have not yet been understood.

If $\sigma(\text{Si}=\text{Si}) \rightarrow \pi^*(\text{Si}=\text{Si})$ coupling is responsible for the shifts of both Si centers, the energy denominator of this excitation has to be the same in both cases and cannot account for the observed differences. To achieve a better

understanding of the substituent effects on ²⁹Si shifts in both symmetrically and unsymmetrically substituted disilenes, we have now carried out a quantum chemical analysis of the individual contributing terms in the sum-over-states expression (eq 1) for σ^p . The analysis method implemented for this purpose allows a breakdown of σ^p into individual contributions by occupied and unoccupied molecular orbitals (MOs) within a density functional theory (DFT) framework. As described in the following, this breakdown has been performed in unprecedented detail.

Theoretical Background

When using a wave function Ψ_0 that consists of a single Slater determinant of molecular orbitals (MOs), as in Hartree–Fock or density functional theories, we may rewrite eq 1 as a double sum over occupied and virtual molecular orbitals ϕ_k and ϕ_a , respectively (u and v represent Cartesian components):²⁰

$$\sigma_{N,uv}^p = \frac{2}{c^2} \sum_k \sum_a \frac{\text{occ vac} \langle \phi_k | I_{O,u} | \phi_a \rangle \cdot \langle \phi_a | I_{N,v} \cdot r_N^{-3} | \phi_k \rangle}{\Delta E_{k \rightarrow a}} \quad (2)$$

In the case of local (LDA) or gradient-corrected (GGA) density functional calculations, the energy denominators simplify further to differences between occupied and virtual Kohn–Sham orbital energies (uncoupled DFT – UDFT²²), whereas coupling terms have to be taken into account in the case of Hartree–Fock or hybrid-DFT calculations.²³ Note that eq 2 refers to a common gauge origin, but it can be extended easily for other choices of gauge.^{23,24}

Depending on the computational framework used, the occupied orbitals entering eq 2 may either be localized MOs or canonical MOs, whereas the virtual MOs are normally always taken to be canonical, i.e., delocalized. Analyses of eq 2 in terms of localized occupied MOs are usually carried out when using individual gauges for localized orbitals (IGLO) to treat the gauge problem.²³ We have initially carried out a DFT-IGLO-based analysis. However, the results did not allow us to understand the substituent effects adequately, as the relation to the energy denominators is not straightforward anymore. Subsequently, we have attempted the analysis in terms of canonical MOs, within the framework of gauge-including atomic orbitals (GIAOs).²⁴ While this analysis provides a better connection to the energy denominators, the GIAO method involves additional contributions to the sum-over-states expression in eq 2, due to gauge-dependent couplings among the occupied MOs. Unfortunately, these terms, which are difficult to interpret chemically, turned out to change significantly from system to system, thus complicating the picture. We have therefore decided to carry out the final analyses with canonical MOs and a common, single gauge origin at the midpoint of the two central silicon atoms. While

(18) Ramsey, N. F. *Phys. Rev.* **1950**, *78*, 699.

(19) Kaupp, M.; Malkina, O. L.; Malkin, V. G.; Pyykkö, P. *Chem. Eur. J.* **1998**, *4*, 118, and references therein.

(20) L_O represents angular momentum around the gauge origin of the external vector potential due to the external magnetic field, and L_N represents angular momentum around the nucleus in question. Both of these operators may be expressed as a sum over one-electron operators I_O and I_N , respectively. Equation 1 uses cgs-based atomic units, and c is the speed of light. OZ matrix elements are later on provided in mHartree/Zeeaman (1 Hartree = 27.2116 eV, 1 Zeeman = 2.4×10^5 T), and PSO matrix elements in 10^{-3} Zeeman.

(21) ²⁹Si NMR shifts of further unsymmetrical disilene systems (see also ref 13) ($(\text{Bu}_2\text{Me})_2\text{Si}=\text{Si}(\text{Mes})_2$: 148.6 ppm for $(\text{Mes})_2\text{Si}$; 8.2 ppm for $(\text{Bu}_2\text{MeSi})_2\text{Si}$; $(\text{Pr}_3\text{Si})_2\text{Si}=\text{Si}(\text{Is})_2$ (Is = 2,4,6-triisopropylphenyl): 137.2 ppm for $(\text{Is})_2\text{Si}$; 14.0 ppm for $(\text{Pr}_3\text{Si})_2\text{Si}$; $(\text{Bu}_2\text{Me})_2\text{Si}=\text{Si}(\text{Is})_2$: 142.0 ppm for $(\text{Is})_2\text{Si}$; 14.9 ppm for $(\text{Bu}_2\text{MeSi})_2\text{Si}$).

(22) Malkin, V. G.; Malkina, O. L.; Eriksson, L. A.; Salahub, D. R. In *Modern Density Functional Theory: A Tool for Chemistry*; Seminario, J. M., Politzer, P., Eds.; Elsevier: Amsterdam, 1995; Vol. 2, pp 273–347.

(23) Kutzelnigg, W.; Fleischer, U.; Schindler, M. In *NMR—Basic Principles and Progress*; Diehl, P., Fluck, E., Günther, H., Kosfeld, R., Eds.; Springer-Verlag: Heidelberg, 1990; Vol. 23, p 165.

(24) Wolinski, K.; Hilton, J. F.; Pulay, P. *J. Am. Chem. Soc.* **1990**, *112*, 8251, and references therein.

the basis-set convergence in such single-gauge calculations is inferior to IGLO or GIAO calculations, we found that with the extended basis sets used (see below), the relevant deviations from the GIAO results are acceptable and do not affect the final conclusions of the analyses.

To our knowledge, only Schreckenbach, Ziegler, and co-workers have previously carried out detailed MO analyses of chemical shieldings in terms of canonical MOs, within a DFT-GIAO framework and for transition metal complexes.²⁵ We go beyond these studies by analyzing in detail for each term in the sum-over-states expression (eq 2) not only the overall contribution to σ^p and the energy denominator but also the individual OZ and PSO matrix elements in the numerators, to obtain further insight. In particular, the PSO term (second matrix element) involves the electron–nucleus distance to the third power in the denominator. It is therefore extremely sensitive to finer details of the electron density distribution around the nucleus in question. We note in passing that the breakdown into individual matrix elements is to some extent gauge dependent. Occasionally, the sign of a matrix element may be ill-defined, due to off-diagonal contributions. However, we have convinced ourselves that the main conclusions of the analyses are not affected by these details.

Computational Details

Structure optimizations and harmonic vibrational frequency analyses (to establish the nature of stationary points on the potential energy surface) were performed at the HF/6-31+G(d), B3LYP/6-31+G(d),²⁶ and MP2/6-31+G(d) level,²⁷ using the *Gaussian98* program package.²⁸ Optimization of **1** and **2** used C_{2h} symmetry, that of **3** C_s symmetry, while **4** and **5** had to be optimized without symmetry. Natural population analyses²⁹ employed the built-in NBO-3.0 subroutines of the *Gaussian98* program. Chemical shifts were initially calculated with *Gaussian98* at the HF-GIAO and BP86-GIAO gradient-corrected DFT level,^{24,30} using the extended IGLO-III basis sets of Kutzelnigg et al.²³ Calculated absolute shieldings σ were converted to relative shifts δ via calculated shieldings for tetramethylsilane (TMS) at the same levels [$\sigma_{\text{calc}}(\text{Si}) = 390.0$ ppm for HF-GIAO/IGLO-III/B3LYP/6-31+G(d), 326.0 ppm for BP86-GIAO/IGLO-III/B3LYP/6-31+G(d), 389.3 ppm for HF-GIAO/IGLO-III/MP2/6-31+G(d), and 327.5 ppm for BP86-

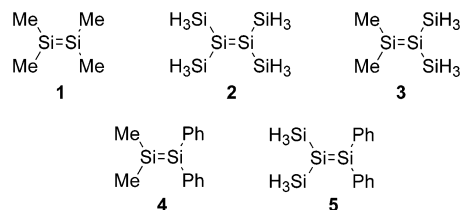


Figure 2. Selected disilene model systems.

GIAO/IGLO-III/MP2/6-31+G(d) levels]. Isotropic shieldings and shifts are the average of the three principal tensor components.

Subsequent analyses of the individual contributions to σ^p for **1–3** were carried out at the BP86/IGLO-III level, using the MP2-optimized structures. We used Kohn–Sham orbitals obtained at this level with *Gaussian98* and transferred them to the in-house property program *MAG-ReSpect*,^{31,32} using a recently implemented interface routine.³³ With *MAG-ReSpect*^{31,32} it is possible to calculate nuclear shieldings at Hartree–Fock and pure or hybrid DFT levels using IGLO, GIAO, or single-origin methods. The program has been extended for this study to enable a detailed breakdown of eq 2 into individual terms in the sum-over-states expression.

Results and Discussion

Structure Optimizations. A variety of symmetrically and unsymmetrically substituted model systems has been examined (Figure 2). Both calculations³⁴ and experiments¹⁷ indicate that symmetrical disilenes exist as trans-bent equilibrium structures. As has been shown previously,^{17,34} inclusion of electron correlation is required to reproduce the structural parameters of disilenes, but MP2 and B3LYP-DFT methods provide comparable accuracy. This is confirmed for our model systems **1–3** in Table 1, where MP2 and B3LYP structures agree well with each other but deviate significantly from the Hartree–Fock-optimized structures.

Interestingly, the unsymmetrically substituted model systems **3** and **5** exhibit a significantly larger pyramidalization at the silyl-substituted center [Si(1)] than at the methyl- or phenyl-substituted center [Si(2)], which is in contrast to the situation for the symmetrically substituted systems. This may be rationalized when considering the natural charge distribution computed for **3** (Figure 3): The silyl-substituted “silylene” fragment obtains a negative partial charge. Following the CGMT (Carter–Goddard–Malrieu–Trinquier)³⁵ donor–acceptor model, the methyl-substituted fragment acts

(25) See, e.g.: Ruiz-Morales, Y.; Schreckenbach, G.; Ziegler, T. *J. Phys. Chem.* **1996**, *100*, 3359. Gilbert, T. M.; Ziegler, T. *J. Phys. Chem. A* **1999**, *103*, 7535.

(26) (a) Becke, A. D. *J. Chem. Phys.* **1993**, *98*, 5648. (b) Lee, C.; Yang, W.; Parr, R. G. *Phys. Rev. B* **1988**, *37*, 785.

(27) Differences between the results of MP2/6-311++G(d,p) and MP2/6-31+G(d) calculations of model system **1** are 0.5 pm for Si=Si, 0.7 pm for the Si–C bond length, and 0.1° in pyramidalization. The trans-bent structure is reproduced at any of these levels.

(28) Frisch, M. J.; Trucks, G. W.; Schlegel, H. B.; Scuseria, G. E.; Robb, M. A.; Cheeseman, J. R.; Zakrzewski, V. G.; Montgomery, J. A., Jr.; Stratmann, R. E.; Burant, J. C.; Dapprich, S.; Millam, J. M.; Daniels, A. D.; Kudin, K. N.; Strain, M. C.; Farkas, O.; Tomasi, J.; Barone, V.; Cossi, M.; Cammi, R.; Mennucci, B.; Pomelli, C.; Adamo, C.; Clifford, S.; Ochterski, J.; Petersson, G. A.; Ayala, P. Y.; Cui, Q.; Morokuma, K.; Malick, D. K.; Rabuck, A. D.; Raghavachari, K.; Foresman, J. B.; Cioslowski, J.; Ortiz, J. V.; Stefanov, B. B.; Liu, G.; Liashenko, A.; Piskorz, P.; Komaromi, I.; Gomperts, R.; Martin, R. L.; Fox, D. J.; Keith, T.; Al-Laham, M. A.; Peng, C. Y.; Nanayakkara, A.; Gonzalez, C.; Challacombe, M.; Gill, P. M. W.; Johnson, B. G.; Chen, W.; Wong, M. W.; Andres, J. L.; Head-Gordon, M.; Replogle, E. S.; Pople, J. A. *Gaussian 98*, revision A.7; Gaussian, Inc.: Pittsburgh, PA, 1998.

(29) (a) Reed, A. E.; Weinhold, F. *J. Chem. Phys.* **1985**, *83*, 1736. (b) Reed, A. E.; Curtiss, L. A.; Weinhold, F. *Chem. Rev.* **1988**, *88*, 899.

(30) (a) Becke, A. D. *Phys. Rev. A*, **1988**, *38*, 3098. (b) Perdew, J. P. *Phys. Rev. B* **1986**, *33*, 8822.

(31) Malkin, V. G.; Malkina, O. L.; Reviakine, R.; Schimmelpfennig, B.; Arbuznikov, A. V.; Kaupp, M. *MAG-ReSpect*, version 1.0; 2002.

(32) (a) This version of *MAG-ReSpect* uses the integral package of *DALTON*. (b) Helgaker, T.; Jensen, H. J. Aa.; Jørgensen, P.; Olsen, J.; Ruud, K.; Agren, H.; Auer, A. A.; Bak, K. L.; Bakken, V.; Christiansen, O.; Coriani, S.; Dahle, P.; Dalskov, E. K.; Enevoldsen, T.; Fernandez, B.; Hättig, C.; Hald, K.; Halkier, A.; Heiberg, H.; Hettema, H.; Jonsson, D.; Kirpekar, S.; Kobayashi, R.; Koch, H.; Mikkelsen, K. V.; Norman, P.; Packer, M. J.; Pedersen, T. B.; Ruden, T. A.; Sanchez, A.; Saue, T.; Sauer, S. P. A.; Schimmelpfennig, B.; Sylvester-Hvid, K. O.; Taylor, P. R.; Vahtras, O. *DALTON*, Release 1.2, 2001.

(33) (a) Reviakine, R. *Gaussian-to-MAG interface*, version 1.0, 2002. (b) Kaupp, M.; Reviakine, R.; Malkina, O. L.; Arbuznikov, A.; Schimmelpfennig, B.; Malkin, V. G. *J. Comput. Chem.* **2002**, *23*, 794.

(34) Takahashi, M.; Sakamoto, K. *Organometallics* **2002**, *21*, 4212, and references therein.

(35) (a) Trinquier, G.; Malrieu, J.-P. *J. Am. Chem. Soc.* **1987**, *109*, 5303. (b) Malrieu, J.-P.; Trinquier, G. *J. Am. Chem. Soc.* **1989**, *111*, 5916. (c) Trinquier, G. *J. Am. Chem. Soc.* **1990**, *112*, 2130. (d) Trinquier, G.; Malrieu, J.-P. *J. Phys. Chem.* **1990**, *94*, 6184.

Table 1. Computed Structural Parameters at Different Computational Levels^a

| model | method | bond length | | | pyramidity ^b | |
|----------|--------|-------------|-----------------|-----------------|-------------------------|-----------|
| | | r(Si=Si) | r(Si-Si) | r(Si-C) | Si(1)(Si) | Si(2)(C) |
| 1 | B3LYP | 218.8 | | 190.2 | | 351.0 |
| | MP2 | 218.1 | | 189.3 | | 351.5 |
| | HF | 214.3 | | 189.4 | | 357.5 |
| 2 | B3LYP | 217.4 | 234.5 | | 359.5 | |
| | MP2 | 217.8 | 233.4 | | 356.7 | |
| | HF | 215.4 | 235.1 | | 359.9 | |
| 3 | B3LYP | 218.5 | 234.1 | 189.2 | 346.8 | 357.1 |
| | MP2 | 217.9 | 232.9 | 188.4 | 344.2 | 357.1 |
| | HF | 215.1 | 233.9 | 188.7 | 358.9 | 359.6 |
| 4 | B3LYP | 218.7 | | Me: 189.8,189.9 | | Me: 352.8 |
| | | | | Ph: 188.1,188.1 | | Ph: 353.7 |
| 5 | B3LYP | 219.3 | 234.2, 234.3 | 187.4,187.5 | 348.3 | 357.7 |

^a With 6-31+G(d) basis sets. Bond lengths in pm, angles in deg. ^b Sum of angles around silicon center.

Table 2. Computed ²⁹Si Chemical Shift Tensors (in ppm vs TMS)^a

| model | method | δ ₁ ^b | δ ₂ ^b | δ ₃ ^b | δ _{iso} |
|--|----------|-----------------------------|-----------------------------|-----------------------------|------------------|
| 1 | HF | 274.6 (268.8) | 72.9 (70.0) | 15.4 (15.1) | 121.0 (118.0) |
| | BP86-DFT | 282.1 (279.9) | 88.0 (85.8) | 3.8 (5.2) | 124.6(123.6) |
| 2 | HF | 474.4 (507.1) | 65.7 (73.1) | -94.9 (-101.6) | 148.4 (159.5) |
| | BP86-DFT | 418.1 (445.7) | 92.8 (106.2) | -101.6 (-107.5) | 136.0 (148.2) |
| 3 [Si(SiH ₃) ₂] | HF | 128.4 (124.2) | -85.9 (-95.9) | -113.5 (-121.7) | -23.7 (-31.1) |
| | BP86-DFT | 139.2 (137.8) | -62.3 (-70.6) | -124.3 (-131.2) | -15.8 (-21.3) |
| 3 (SiMe ₂) | HF | 572.3 (587.7) | 116.6 (116.4) | 39.0 (39.2) | 242.6 (247.8) |
| | BP86-DFT | 534.5 (550.8) | 139.6 (141.6) | 24.8 (25.8) | 233.0 (239.4) |
| 4 (SiMe ₂) | HF | 220.0 | 92.0 | 12.2 | 108.1 |
| | BP86-DFT | 242.4 | 118.5 | 0.0 | 120.3 |
| 4 (SiPh ₂) | HF | 233.1 | 75.9 | 20.3 | 109.7 |
| | BP86-DFT | 245.5 | 84.2 | 7.2 | 112.3 |
| 5 [Si(SiH ₃) ₂] | HF | 70.6 | -79.5 | -124.1 | -44.3 |
| | BP86-DFT | 102.4 | -31.1 | -143.1 | -23.9 |
| 5 (SiPh ₂) | HF | 516.3 | 71.9 | 53.2 | 213.8 |
| | BP86-DFT | 475.6 | 87.0 | 33.8 | 198.8 |

^a GIAO results obtained with Gaussian 98 and IGLO-III basis sets. Results for B3LYP-optimized structures, with results for MP2-optimized structures in parentheses. ^b δ₁ is oriented in z-direction, δ₂ along y-direction, and δ₃ along x-direction.

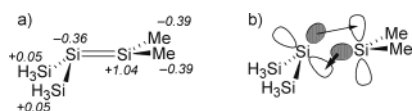


Figure 3. (a) Calculated natural charges for central silicon atoms and substituents in **3**. Silylene fragment charges are (H₃Si)₂Si -0.26; Me₂Si +0.26. (b) Approximate bonding scheme for **3**.

more as a donor and less as an acceptor, and the silyl-substituted fragment is a net electron acceptor. Electrostatic preferences may be responsible for this behavior. As Figure 3a shows, the unequal charge transfer contributes to a favorable alternation of negative and positive charges. Consequently, the central atom Si(1) of the “net acceptor” fragment is significantly pyramidalized, whereas the central atom Si(2) of the “net donor” fragment is almost planar (Figure 3b). However, we note that complete planarization of **3** requires only ca. 2 kJ mol⁻¹ at the B3LYP/6-31+G(d) level.

Chemical Shift Tensors. Table 2 shows that computed NMR chemical shift tensors for **1–3** with MP2- and B3LYP-optimized structures agree well, and thus we could use the more convenient B3LYP-optimizations for the larger models **4** and **5**. The table compares also HF-GIAO and BP86-GIAO methods for the chemical shifts. While there are some discrepancies between the two levels, in particular for δ₁₁, the overall results are similar regarding the substituent effects. As the UDFT calculations with the BP86 functional allow the energy denominators in eq 2 to be identified with the Kohn–

Table 3. Influence of Gauge Treatment on ²⁹Si Shielding Tensors (in ppm)^a

| model | gauge | σ ₁ | σ ₂ | σ ₃ | σ _{iso} |
|--|-------|----------------|----------------|----------------|------------------|
| 1 | GIAO | 52.3 | 248.4 | 329.9 | 210.2 |
| | CGO | 53.1 | 239.5 | 329.4 | 207.3 |
| 2 | GIAO | -107.0 | 233.1 | 445.0 | 190.4 |
| | CGO | -90.1 | 242.9 | 479.4 | 210.8 |
| 3 [Si(SiH ₃) ₂] | GIAO | 194.0 | 408.4 | 465.6 | 356.0 |
| | CGO | 208.4 | 416.3 | 490.3 | 371.7 |
| 3 (SiMe ₂) | GIAO | -213.5 | 192.7 | 310.7 | 96.6 |
| | CGO | -211.7 | 187.7 | 319.1 | 98.4 |

^a MAG-ReSpect results at BP86/IGLO-III level.

Sham orbital energy differences, it is more convenient to base our further analyses for **1–3** on the DFT results. As discussed above, neither IGLO nor GIAO treatment provided a completely suitable basis for closer interpretation, and thus we resorted to calculations with a common gauge origin at the midpoint of the Si=Si bond. Table 3 shows that the differences in the shielding tensors compared to the corresponding GIAO-based calculations are still notable but not anymore dramatic with the extended IGLO-III basis sets used. All trends and substituent effects are faithfully reproduced with a single origin, and thus we may confidently carry out our shielding analyses at this computational level.

Model systems **1–3** were thus further analyzed at the BP86-CGO/IGLO-III//MP2/6-31+G(d) level, using the MAG-ReSpect³¹ program. Contributions to σ^p may be broken down into individual terms of the sum-over-states formula (eq 2), related in each case to the coupling

Table 4. Analysis of the Major Contribution to σ^p Values of **1^a**

| orbital | nr. | contribution | couplings to ^b | direction ^c | ΔE [eV] ^d | OZ | PSO |
|---------|-----|--------------|---------------------------|------------------------|------------------------------|-------|-------|
| | 29 | -112.1 | MO 37: -29.4 | σ_3 | -9.04 | +3.09 | +2.49 |
| | | | MO 44: -48.4 | σ_3 | -9.97 | -5.54 | -2.41 |
| | | | MO 64: -20.9 | σ_3 | -14.38 | +2.72 | +3.20 |
| | | | rest: -13.4 | - | - | - | - |
| | 30 | -207.4 | MO 33: -118.5 | σ_2 | -5.62 | +3.36 | +5.51 |
| | | | MO 36: -21.8 | σ_2, σ_3 | -7.53 | +2.87 | +1.99 |
| | | | MO 48: -51.4 | σ_3 | -9.96 | -4.66 | -3.18 |
| | | | rest: -37.5 | - | - | - | - |
| | 31 | -242.2 | MO 33: -208.7 | σ_1 | -5.09 | -3.91 | -7.84 |
| | | | MO 36: -21.3 | σ_1 | -7.00 | -1.64 | -2.50 |
| | | | MO 61: +29.3 | σ_3 | -12.30 | +3.67 | -2.71 |
| | | | rest: -41.5 | - | - | - | - |
| | 32 | -98.6 | MO 34: -78.4 | σ_2 | -3.77 | +2.26 | +3.70 |
| | | | MO 47: -23.6 | σ_1 | -6.79 | +1.98 | +2.24 |
| | | | MO 53: +19.6 | σ_2 | -7.62 | +1.54 | -2.75 |
| | | | rest: -16.2 | - | - | - | - |

^a Schematical drawings of selected MOs; selected isosurface plots see Figure 4. Shielding contributions in ppm, OZ matrix elements in mHartree/Zeeman, PSO matrix elements in mZeeman. ^b Selection of the three largest contributions. ^c Main direction to which this coupling contributes. ^d $\Delta E = E_0 - E_n$.

Table 5. Analysis of the Major Contributions to σ^p in **2^a**

| orbital ^a | nr. | contribution | couplings to ^b | direction ^c | ΔE [eV] ^d | OZ | PSO |
|----------------------|-----|--------------|---------------------------|------------------------|------------------------------|-------|-------|
| | 45 | -99.4 | MO 50: -21.4 | σ_3 | -6.09 | +1.63 | +2.27 |
| | | | MO 53: -42.9 | σ_3 | -6.87 | -4.64 | -1.80 |
| | | | MO 61: -20.5 | σ_2 | -8.35 | -2.77 | -1.81 |
| | | | rest: -14.6 | - | - | - | - |
| | 46 | -280.3 | MO 49: -290.5 | σ_1 | -3.94 | -4.32 | -7.29 |
| | | | MO 64: +55.1 | σ_3 | -8.45 | -3.23 | +3.98 |
| | | | MO 66: -29.8 | σ_3 | -9.14 | -2.68 | -2.80 |
| | | | rest: -15.1 | - | - | - | - |
| | 47 | -253.7 | MO 49: -169.7 | σ_2 | -3.68 | +3.22 | +5.36 |
| | | | MO 51: -49.9 | σ_3 | -5.48 | -5.87 | -1.35 |
| | | | MO 57: -29.3 | σ_3 | -7.15 | -2.03 | -2.85 |
| | | | rest: -4.8 | - | - | - | - |
| | 48 | -68.8 | MO 52: -39.0 | σ_2 | -4.03 | +1.27 | +3.50 |
| | | | MO 62: +20.8 | σ_2 | -6.51 | +1.37 | -2.85 |
| | | | MO 84: -32.2 | σ_1 | -10.75 | +2.72 | +3.50 |
| | | | rest: -18.4 | - | - | - | - |

^a Schematical drawings of selected MOs. Shielding contributions in ppm, OZ matrix elements in mHartree/Zeeman, PSO matrix elements in mZeeman. ^b Selection of the three largest contributions. ^c Main direction to which this coupling contributes. ^d $\Delta E = E_0 - E_n$.

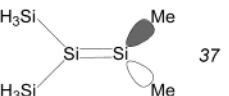
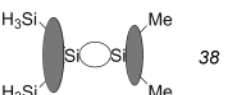
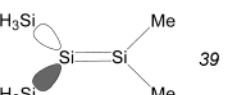
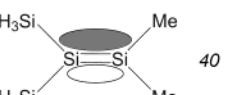
of exactly one occupied to one virtual MO. We first of all have to remark that the dominant contributions in each case arise from couplings of the four occupied MOs at highest energy to virtual MOs. These occupied MOs are sketched in Tables 4–6 and are shown in more detail as isosurface plots [together with the $\pi^*(\text{Si}=\text{Si})$ LUMO], for tetramethyldisilene (**1**) in Figure 4 and for 1-disilyl-2-dimethyldisilene (**3**) in Figure 5. For reasons of clarity, the tables generally list only the major contributions to σ^p .

In **1**, two out of these four MOs dominate σ^p : orbital 30, which is mainly $\sigma(\text{Si}-\text{C})$ bonding and orbital 31, which corresponds largely to the $\sigma(\text{Si}=\text{Si})$ bond. Magnetic couplings of these MOs are not restricted to just one unoccupied MO but are distributed over a number of appropriate combinations. For a large contribution

to σ^p , (a) the energy denominator in one of the terms in eq 2 has to be sufficiently small, and (b) both matrix elements in the numerator have to be sufficiently large. The latter requires that angular momentum (present in both OZ and PSO operators) transforms an occupied MO to a form that overlaps well with the appropriate unoccupied MO. This corresponds to a paramagnetic ring current in the plane containing the two MOs involved, and the corresponding major contribution to σ^p points perpendicular to this plane. In other words, preferred rotation around an axis leads to large σ^p contributions along this axis.

In model system **1** this can be illustrated easily, e.g., by comparing the occupied MO 30 to the LUMO 33 (Figure 4). Rotation of 30 (antisymmetric combination of Si-C σ -bonding MOs) around the Si=Si bond (y -axis)

Table 6. Analysis of the Major Contributions to σ^p in **3**^a

| Si(1) (SiH ₃ -substituted) | | | | | | Si(2) (CH ₃ -substituted) | | | | | | | |
|---------------------------------------|---------------|-----------------|------------------------|-------|--------------------|---|-------|--------|---------------|-----------------|------------------------|-------|-------|
| contr. | couplings to | ΔE [eV] | direction ^b | OZ | PSO | orbital | nr. | contr. | couplings to | ΔE [eV] | direction ^b | OZ | PSO |
| +2.8 | MO 41: +18.8 | -5.62 | σ_2 | +2.19 | -1.36 ^d |  | 37 | -319.6 | MO 41: -127.2 | -5.62 | σ_2 | +2.19 | +9.00 |
| | MO 49: -8.00 | -9.10 | σ_2, σ_3 | +2.81 | +0.72 | | | | MO 54: -53.5 | -9.85 | σ_3 | +4.41 | +3.36 |
| | MO 73: -8.96 | -13.5 | σ_3 | -2.17 | -1.63 | rest: -107.8 | - | | - | - | - | | |
| | rest: +0.96 | - | - | - | - | MO 41: -278.4 | -4.49 | | σ_1 | -4.06 | -8.48 | | |
| -174.2 | MO 41: -200.3 | -4.49 | σ_1 | -4.06 | -6.11 |  | 38 | -312.4 | MO 74: -22.3 | -12.94 | σ_3 | +2.20 | +3.76 |
| | MO 48: +23.2 | -7.61 | σ_3 | +2.30 | -2.12 | | | | MO 108: +13.0 | -21.41 | σ_3 | +1.57 | -5.33 |
| | MO 74: -36.3 | -12.94 | σ_3 | +2.20 | +5.95 | rest: -24.7 | - | | - | - | - | | |
| | rest: +39.2 | - | - | - | - | MO 41: -29.8 | -4.38 | | σ_2 | +2.51 | +1.50 ^d | | |
| -286.9 | MO 41: -133.9 | -4.38 | $\sigma_2, (\sigma_3)$ | +2.51 | +6.45 |  | 39 | -41.2 | MO 42: +5.80 | -5.83 | σ_3 | -3.77 | +0.34 |
| | MO 42: -82.5 | -5.83 | σ_3 | -3.77 | -3.52 | | | | MO 54: -4.74 | -8.61 | σ_3 | -1.89 | -0.60 |
| | MO 51: -42.9 | -8.23 | σ_2, σ_3 | +2.24 | +4.53 | rest: -12.46 | - | | - | - | - | | |
| | rest: -27.6 | - | - | - | - | MO 43: -45.2 | -4.05 | | σ_2 | +1.67 | +3.16 | | |
| -73.4 | MO 43: -58.2 | -4.05 | σ_2 | +1.67 | +3.89 |  | 40 | -78.0 | MO 50: +15.0 | -6.13 | σ_2 | -1.24 | +2.14 |
| | MO 47: +21.7 | -5.43 | σ_1 | +1.48 | -2.20 | | | | MO 55: -30.8 | -6.87 | σ_1 | +1.85 | +3.16 |
| | MO 73: -25.4 | -10.36 | σ_1 | +0.98 | +7.36 | rest: -17.0 | - | | - | - | - | | |
| | rest: -11.5 | - | - | - | - | | | | | | | | |

^a Schematical drawings of selected MOs; selected isosurface plots see Figure 5. Shielding contributions in ppm, OZ matrix elements in mHartree/Zeeman, PSO matrix elements in mZeeman. ^b Main direction to which this coupling contributes. ^c $\Delta E = E_0 - E_r$. ^d Sign of PSO term corrected after calculation.

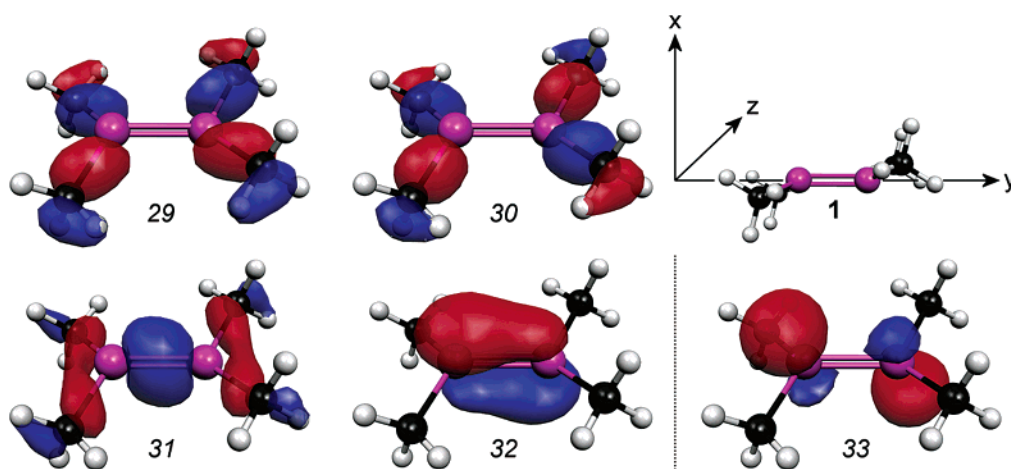


Figure 4. Isosurface plots (± 0.06 au) of selected MOs for model system **1**.³⁶

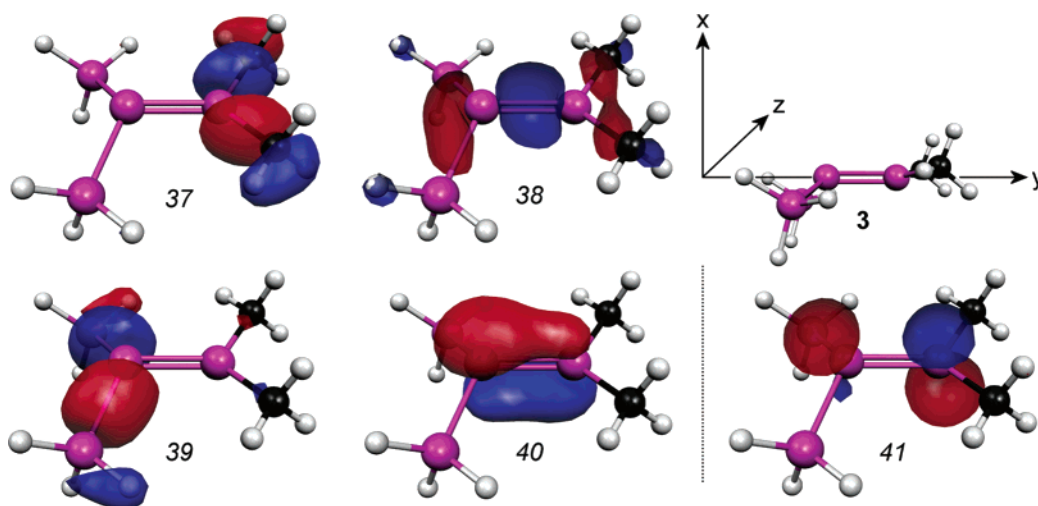


Figure 5. Isosurface plots (± 0.06 au) of selected MOs for model system **3**.³⁶

produces a transformed MO that matches nicely with the LUMO 33. As the corresponding energy denominator is relatively small (-5.62 eV; Table 4), this coupling

leads to a significant deshielding contribution along the y -axis (σ_2 ; cf. Table 4). While the symmetric MO 29 is only slightly lower in energy than 30, it has the wrong

nodal structure to interact properly with **33** when rotated in the xz -plane. Thus the corresponding sum-over-states term is negligibly small (<1 ppm).

The overall largest individual coupling is the one between the $\sigma(\text{Si}=\text{Si})$ bonding MO **31** and LUMO **33**. As the corresponding rotation (ring current) is around the z -axis, this term contributes mainly along z (σ_1). This is the term on which previous analyses focused.¹⁷ Indeed, the corresponding $\sigma(\text{Si}=\text{Si}) \rightarrow \pi^*(\text{Si}=\text{Si})$ coupling for tetrasilyldisilene **2**, $46 \rightarrow 49$ (Table 5), is larger and thus to a large extent responsible for the larger deshielding (again via σ_1). While the product of the OZ and PSO matrix elements for this coupling is also slightly larger in **2** than in **1**, the main difference between the two systems is caused by the smaller energy denominator [$\Delta E(31 \rightarrow 33)$ in **1**: 5.09 eV, $\Delta E(46 \rightarrow 49)$ in **2**: 3.94 eV; see also Tables 4 and 5], due to the lower energy of **49** (-3.20 eV) in **2** compared to that of **33** (-1.76 eV) in **1**. This is consistent with the main conclusions reached by West et al.,¹⁷ who attributed the substituent effects on the ^{29}Si shifts in disilenes mainly to a reduction of the energy denominator for this coupling by electro-positive substituents. However, closer comparison of Tables 4 and 5 shows that the $47 \rightarrow 49$ coupling in **2** is enhanced even more compared to the equivalent $30 \rightarrow 33$ coupling in **1** (again due to a reduced energy denominator, thus enhancing deshielding contributions mainly along σ_2). Other contributions change as well. As another result, σ_3 is decreased almost by the same amount as σ_1 is increased, and σ_{iso} for the two compounds **1** and **2** differs much less than σ_1 might suggest (Table 3).

The situation changes dramatically for the unsymmetrical 1-disilyl-2-dimethyldisilene (**3**). The most striking spectroscopic result for $(\text{Mes})_2\text{Si}=\text{Si}(\text{Si}^i\text{Pr}_3)_2$,¹¹ the large difference in the isotropic shifts of the two central silicon nuclei, is well simulated by **3**, where the center on the silyl-substituted side [Si(1)] is almost 200 ppm more shielded than that on the methyl-substituted side [Si(2)] (Table 3). This constitutes an opposite relative behavior than observed for the silyl- and methyl-substituted centers in the symmetrical derivatives **1** and **2**.

It becomes immediately obvious from Table 6 that we may not argue via different energy denominators for the different sites. The interacting orbitals are identical, and so are their energy denominators. While the differences in σ_1 are again most pronounced, those for σ_2 and σ_3 are by no means negligible. Concentrating first on σ_1 , we note that the major coupling is again that between the $\sigma(\text{Si}=\text{Si})$ bonding combination **38** and the $\pi^*(\text{Si}=\text{Si})$ antibonding LUMO **41** (Table 6). As the energy denominator for this coupling must be identical for both Si(1) and Si(2) sites, we have to focus on the matrix elements in the numerator of eq 2. The OZ matrix element is also identical (it describes the interaction of the MOs with the external magnetic field), and thus it is the larger PSO matrix element at the Si(2) site that is responsible for the much larger contribution from $38 \rightarrow 41$ coupling at the methyl-substituted end. The PSO matrix element represents interaction with the nuclear magnetic moment on a given NMR nucleus, and due to its r^{-3} dependence the PSO operator samples mainly the local environment of that nucleus (more precisely, the inner-

core tails of the valence MOs at this center). From a local perspective both MOs **38** and **41** look indeed very different at both sites (Figure 5): While MO **38** is very little polarized, the LUMO **41** is strongly concentrated on the Si(2) side (Figure 5). This leads to a much larger PSO term and thus larger deshielding at the Si(2) site, not only for the $38 \rightarrow 41$ coupling, but also for other couplings (see Table 6).

The asymmetry of the charge distribution in **3** (see also Figure 3) is also reflected in the occupied MOs (Figure 5). For example, the Si-substituent σ -bonding MOs are now strongly polarized, with MO **39** mainly $\sigma[\text{Si}(1)-\text{SiH}_3]$ bonding and MO **37** almost exclusively $\sigma[\text{Si}(2)-\text{CH}_3]$ bonding (Table 6). Consequently, the contributions from these MOs to σ^{P} are very different for the two sites: MO **39** contributes mainly to the deshielding of Si(1) and MO **37** to Si(2) deshielding (via σ_2 and σ_3). In both cases, it is again the PSO matrix element that is responsible for the differences, as it samples the asymmetric charge distribution from a local point of view (energy denominators and OZ matrix elements for a given coupling must be identical at both sites). As the differences between the sites are larger with MO **37**, the overall consequence is a larger deshielding of Si(2). Together with the contributions of MO **38**, which go in the same direction (see above), the much larger deshielding of Si(2) compared to Si(1) results. We note in passing that couplings that are strongly off-center may produce negative PSO matrix elements and thus positive contributions to σ^{P} , as shown for example for the $37 \rightarrow 41$ coupling at the Si(1) site in **3** (Table 6).³⁷

Conclusions

Detailed quantum-chemical analyses of the ^{29}Si chemical shift tensors in substituted disilenes show a more differentiated picture of the substituent effects on shielding than previous studies. We confirm the overriding importance of the energy denominators in the expression for σ^{P} (eq 2) in symmetrically substituted disilenes such as **1** or **2** on their chemical shifts.¹⁷ However, it has become apparent that it is not only the $\sigma(\text{Si}=\text{Si}) \rightarrow \pi^*(\text{Si}=\text{Si})$ coupling that accounts for the substituent effects, but orbitals with σ -bonding character to the substituents make notable contributions as well.

The situation is very different for the shifts of the two Si centers in unsymmetrically substituted disilenes. Here the energy denominators are identical for the two sites and cannot explain the very different shifts. It turns out that the asymmetric charge distribution is reflected in both occupied and unoccupied MOs. This charge asymmetry is sampled efficiently by the nuclear magnetic moments (PSO matrix elements) on the respective silicon nuclei. As a result, the dimethyl-substituted silicon center [Si(2)] in 1-disilyl-2-dimethyl-

(36) (a) Flükiger, P.; Lüthi, H. P.; Portmann, S.; Weber, J. *MOLEKEL* 4.3; Swiss Center for Scientific Computing: Manno, Switzerland, 2000–2002. (b) Portmann, S.; Lüthi, H. P. *CHIMIA* **2000**, 54, 766.

(37) The most famous cases of shielding off-center paramagnetic currents are the low-frequency ^1H shifts of certain transition-metal hydrides (see, e.g.: Buckingham, A. D.; Stephens, P. J. *J. Chem. Soc.* **1964**, 2747; Buckingham, A. D.; Stephens, P. J. *J. Chem. Soc.* **1964**, 4583; Ruiz-Morales, Y.; Schreckenbach, G.; Ziegler, T. *Organometallics* **1996**, 15, 3920).

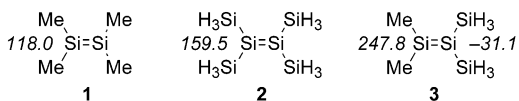


Figure 6. Calculated ²⁹Si NMR shifts of model systems **1–3** [HF-GIAO/IGLO-III//MP2/6-31+G(d)].

disilene (**3**) exhibits more pronounced deshielding than the disilyl-substituted center [Si(1)]. This rationalization of the unexpected shifts in unsymmetrically substituted disilenes increases also the value of ²⁹Si shifts as an analytical tool to distinguish between different systems (see Figure 6).

While this work has concentrated on disilenes, the analysis method used is generally applicable and should be valuable for a better understanding of, for example, structural changes or substituent effects on chemical shifts in a wide variety of molecules. From a chemical point of view it is in particular the possibility of detailed visualization of the magnetically coupled MOs that makes the MO-by-MO analysis of nuclear shieldings,

as carried out here, an attractive tool (see, e.g., comments in ref 38).

Acknowledgment. This study has been supported by Deutsche Forschungsgemeinschaft via the Graduiertenkolleg 690 "Electron Density–Theory and Experiment" at Universität Würzburg, and by Fonds der Chemischen Industrie.

Supporting Information Available: The tables include the standard orientation, the total energies and the calculated shielding tensors for Si of disilene systems **1–5** as well as MO contributions to σ and σ_p for model systems **1–3**. Further information on the Natural Population Analysis for **3** is given and also an additional summary of experimental ²⁹Si NMR shifts for various disilene systems. This material is available free of charge via the Internet at <http://pubs.acs.org>.

OM030101G

(38) Chesnut, D. B.; Quin, L. B.; Wild, S. B. *Heteroat. Chem.* **1997**, *8*, 451.